The 9th European Congress on Computational Methods in Applied Sciences and Engineering
ECCOMAS Congress 2024
3–7 June 2024, Lisboa, Portugal

A MULTI-LAYERED INTEGRAL APPROACH TO THE DE-ICING PROCESS

H. Beaugendre[1], A. Benoit[2], F. Morency[3] and M. Parisot[2]

[1] University Bordeaux, INRIA, CNRS, Bordeaux INP, IMB, UMR 5251,
33405 Talence, France
heloise.beaugendre@math.u-bordeaux.fr

[2] University Bordeaux, INRIA, IMB, CNRS, UMR 5251,
33405 Talence, France

[2] Mechanical Engineering Department, École de Technologie Supérieure,
Montréal, QC H3C 1K3, Canada

Key words: Shallow water in-flight icing/de-icing model, Multi layered integral approach

Summary. The modification of the shallow water icing model to handle de-icing phenomenon is the main focus of this study. As stated in the original model [1], the runback water is modeled utilizing a lubrication assumption for the water film velocity profile. A constant film temperature $T_f(t, x)$ is then calculated under the thin-film hypothesis. Unlike the simplified icing model, the temperature field within the ice layer $T_{ice}(t, x, z)$ is no longer assumed to be constant. Instead, a temperature profile is utilized, enabling the generation of a static film on the wall when a heat conduction source term from a resistance is present [2]. A Temperature profile $T_s(t, x, z)$ is also used in the static film layer if the model predicts the occurrence of this state. In the energy equation for both the solid ice and liquid portion of the static water film, transverse transfers are not considered, a 1D heat equation is then resolved. An integral approach and proper boundary conditions are used to close the problem. The validity of the integral method deteriorates as the thickness over which vertical integration is performed increases. To avoid this problem, a multi-layer approach is proposed. The thickness of the ice block is then divided into three layers of identical thickness. The purpose of this study is to offer a straightforward and robust method suitable for conducting industrial test cases. The model will first be introduced, followed by a description of the numerical approach. Subsequently, validation test cases will be conducted. Realistic de-icing scenarios will then be designed to evaluate the model [3]. Additionally, non-uniform roughness effects will be examined.

1 INTRODUCTION

When the aircraft is in atmospheric conditions that favor the existence of supercooled droplets (subzero temperatures), it is possible to observe ice accretion on solid structures such as wings and fuselage. In fact, the droplets are in a thermodynamically unstable state, leading to an accumulation of ice at the moment of impact with the aircraft. Depending on the external temperature, several scenarios can occur: rime ice accretion (no liquid water), glaze ice accretion (ice + dynamic liquid water film), and in the case of de-icing, a static water film can form under the ice, see Figure 1.

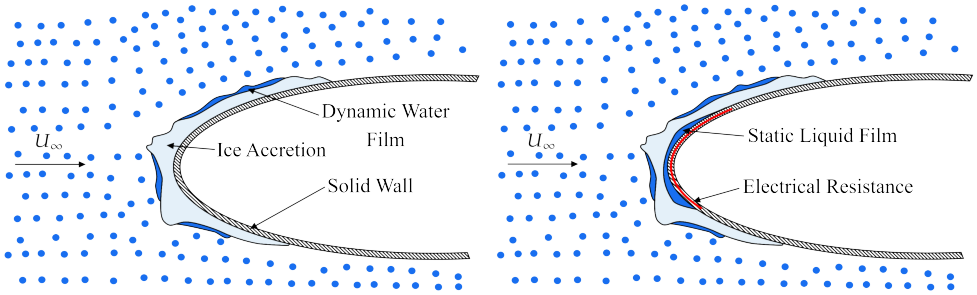

(a) Icing phenomenon. (b) De-icing phenomenon.

Figure 1: Diagram illustrating the phenomenon of icing and de-icing.

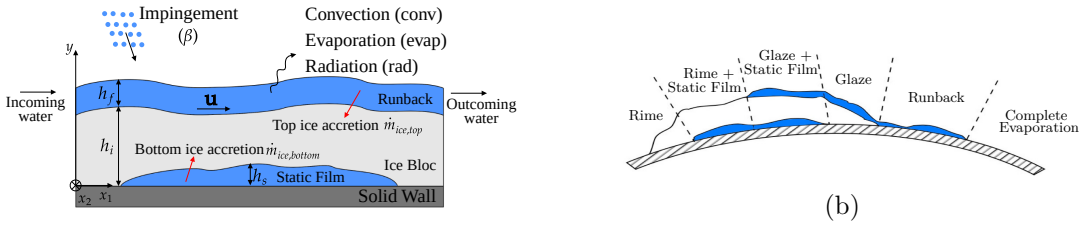

(a) (b)

Figure 2: a) Illustration of the three possible states during de-icing. b) Possible scenarios during de-icing process

During de-icing, water on the wall surface can exist in up to three different states: as a static film of liquid water, as solid ice, or as a runback water film, see Figure 2 a). Figure 2 b) depicts six possible scenarios: rime ice accretion, static film and rime ice accretion, static film and glaze ice accretion, glaze ice accretion, water film runback, and full evaporative case.

2 MATHEMATICAL MODEL

In the more complex scenario, the three states of the water are present and the unknowns of the system of equations (1) are the dynamic film thickness $h_f(t,x)$, the dynamic film temperature $T_f(t,x)$ (No temperature profile is used because the dynamic water film is so thin, typically only a few microns [1]), the instantaneous top ice accretion $\dot{m}_{ice,top}$, the ice thickness $h_i(t,x)$, the ice temperature profile $T_{ice}(t,x,z)$, the instantaneous bottom ice accretion $\dot{m}_{ice,bottom}$, the static film thickness $h_s(t,x)$ and the static film temperature profile $T_s(t,x,z)$. Depending on scenario, the system of equations (1) simplify and specific boundary conditions are applied. Equations (1a) and (1b) are mass and energy conservation for the dynamic water film, respectively. Equation (1c) is mass conservation for the ice block. Equation(1d) is the energy equation inside the ice where it is simplified to the unsteady 1D heat equation [2]. Equation (1e) is the Stefan condition. Equation (1f) is mass conservation for the static film. Finally, equation (1g) is the energy equation inside the static film and also it is simplified to the unsteady 1D heat equation.

$$
\begin{cases}
\dfrac{\partial h_f}{\partial t} + \operatorname{div}(\mathbf{u}\, h_f) = \dfrac{\dot{m}_\beta - \dot{m}_{evap} - \dot{m}_{ice,top}}{\rho_w} & \text{(1a)} \\
\dfrac{h_f T_f}{\partial t} + \operatorname{div}(\mathbf{u}\, h_f T_f) = \dfrac{\dot{Q}_\beta + \dot{Q}_{conv} - \dot{Q}_{evap} - (c_{p,i} T_f - L_f)\dot{m}_{ice,top} - \lambda_i \dfrac{\partial T_{ice}}{\partial z}\Big|_{z=h_i}}{\rho_w c_{p,w}} & \text{(1b)} \\
\rho_i \dfrac{\partial h_i}{\partial t} = \dot{m}_{ice,top} + \dot{m}_{ice,bottom} & \text{(1c)} \\
\rho_i c_{p,i} \dfrac{\partial T_{ice}}{\partial t} = \lambda_i \dfrac{\partial^2 T_{ice}}{\partial z^2} & \text{(1d)} \\
\dot{m}_{ice,bottom} L_f = \lambda_w \dfrac{\partial T_s}{\partial z}\Big|_{z=h_s} - \lambda_i \dfrac{\partial T_{ice}}{\partial z}\Big|_{z=h_i} & \text{(1e)} \\
\rho_w \dfrac{\partial h_s}{\partial t} = -\dot{m}_{ice,bottom} & \text{(1f)} \\
\rho_w c_{p,w} \dfrac{\partial T_s}{\partial t} = \lambda_w \dfrac{\partial^2 T_s}{\partial z^2} & \text{(1g)}
\end{cases}
$$

A parabolic profile with three degrees of freedom is suggested for the temperature distribution, denoted as $T_s(t,x,z)$. The idea of the integral approach is to integrate the temperature over the thickness of the layer and used to obtain an equation for the mean temperature that satisfy the unsteady heat equation.

2.1 Integral approach for the static film

We illustrate the integral approach considering the static film of water. The static film, if it exists, is composed of one layer with a parabolic temperature profile. We define the static film thickness h_s and the mean temperature $\widehat{T}_s$ by (see Fig. 3 a),

$$
\begin{cases}
h_s(t,x) &= z_T(t,x) - z_B(t,x), \\
\widehat{T}_s(t,x) &= \dfrac{1}{h_s(t,x)} \displaystyle\int_{z_B(t,x)}^{z_T(t,x)} T_s(t,x,z)\, dz.
\end{cases} \tag{2}
$$

The Leibniz integral rule applied on the heat equation (Eq. 1g) yields to

$$
\frac{\partial h_s \widehat{T}_s}{\partial t} + T_s\Big|_{z=z_B} \frac{\partial z_B}{\partial t} - T_s\Big|_{z=z_T} \frac{\partial z_T}{\partial t} = \frac{\lambda_w}{\rho_w c_{p,w}} \left[\frac{\partial T_s}{\partial z}\Big|_{z=z_T} - \frac{\partial T_s}{\partial z}\Big|_{z=z_B} \right]. \tag{3}
$$

$T_s(t,x,z)$ is posed as a parabolic profile which respects the boundary conditions and mean temperature field [2],

$$
\begin{aligned}
T_s(t,x,z) &= T_s(t,x,z_B) + 2\left[3\widehat{T}_s(t,x) - 2T_s(t,x,z_B) - T_s(t,x,z_T)\right]\left(\frac{z - z_B(t,x)}{h_s(t,x)}\right) \\
&+ 3\left[T_s(t,x,z_T) + T_s(t,x,z_B) - 2\widehat{T}_s(t,x)\right]\left(\frac{z - z_B(t,x)}{h_s(t,x)}\right)^2.
\end{aligned} \tag{4}
$$

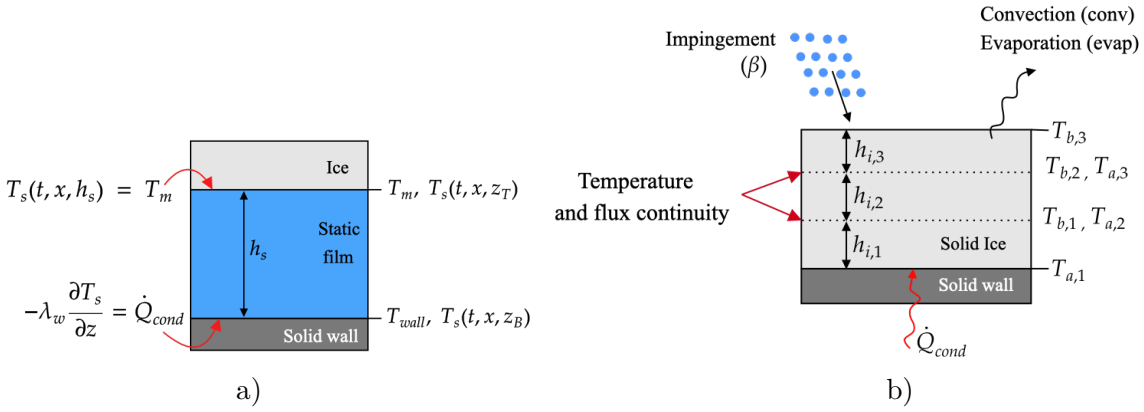

Figure 3: a) Notations for the integral approach. b) Multi-layered approach inside solid ice.

This enables to simplify equation (3) such as

$$\frac{\partial h_s \widehat{T}_s}{\partial t} + T_s(z_B)\dot{z}_B - T_s(z_T)\dot{z}_T = \frac{6\alpha_w}{h_s}\left[T_s(z_B) - 2\widehat{T}_s + T_s(z_T)\right] \tag{5}$$

where $\alpha_w = \dfrac{\lambda_w}{\rho_w c_{p,w}}$, $\dot{z}_B = \dfrac{\partial z_B}{\partial t}$, $\dot{z}_T = \dfrac{\partial z_T}{\partial t}$, $T_s(z_T) = T_s(t,x,z_T)$ and $T_s(z_B) = T_s(t,x,z_B)$. The boundary conditions for the static film are $\dot{z}_B = 0$, $\dot{z}_T = \dfrac{\partial h_s}{\partial t}$, so this yields to equation 6.

$$\frac{\partial h_s \widehat{T}_s}{\partial t} - T_s(z_T)\frac{\partial h_s}{\partial t} = 6\alpha_w \frac{T_s(z_B) - 2\widehat{T}_s + T_s(z_T)}{h_s} \tag{6}$$

The boundary conditions for the temperature profile T_s are

$$-\lambda_w \frac{\partial T_s}{\partial z}\bigg|_{z=z_B} = \dot{Q}_{cond} \tag{7}$$

and $T_s(z_T) = T_m = 273.15\ \mathrm{K} = 0^o\,\mathrm{C}$. Where in Celsius and with equation 4, it gives the temperature at bottom surface

$$T_s(z_B) = \frac{1}{4}\left(\frac{h_s}{\lambda_w}\dot{Q}_{cond} + 6\hat{T}_s\right) \tag{8}$$

An implicit scheme is chosen for $\widehat{T}_s$ and h_s is taken explicit, which equation 6 gives,

$$\widehat{T}_s^{n+1} = \frac{\widehat{T}_s^n(4h_s^n\lambda_w) + 6\Delta t\alpha_w\dot{Q}_{cond}}{(h_s^n)^2 + 3\alpha_w\Delta t}\left(\frac{h_s^n}{4\lambda_w}\right). \tag{9}$$

The equation presented above presents an initialization issue when the static film is in its early stages of formation. To address this, the film temperature is assumed to be constant and equal to T_m during initialization. Prior to the formation of the film, the system is in either the rime ice or glaze ice scenario. The temperature profile within the ice is already established, see sections 2.2 and 2.3. Stefan's equation (1e) is used with boundary condition, equation (7), to determine $\dot{m}_{ice,bottom}$. Equation (1f) is then used to determine the first h_s.

2.2 Multi-layered approach to rime ice

When the layer becomes thick the integral approach fails and may lead to unphysical temperature profile as stated by Chauvin et. al [2]. To overcome this problem, the layer can be subdivided into multiple sub-layers. For example, in this paper the ice block is divided into three layers, and a parabolic profile is applied to each layer. Temperature and flux continuity are imposed between each layer, see Figure 3 b).

The layer of ice, denoted as $h_i(t,x)$, is divided into three identical sublayers each with a thickness of $h(t,x) = \dfrac{h_i(t,x)}{3}$ with $\dfrac{\partial h}{\partial t} = \dfrac{1}{3}\dfrac{\partial h_i}{\partial t}$. In the following, the process is explained for rime ice conditions, as shown in Figure 3 b). If the system state differs, such as rime with static film, glaze with static film, or glaze alone, the boundary conditions will also differ, requiring adjustments to be made. These adjustments will be explained later in sections 2.3 to 2.5.

The boundary conditions for a rime ice situation are

$$\begin{cases} -\lambda_i \dfrac{\partial T_{ice}}{\partial z}\Big|_{z=0} = \dot{Q}_{cond} \\ \\ \lambda_i \dfrac{\partial T_{ice}}{\partial z}\Big|_{z=h_i} = \dot{Q}_\beta + \dot{Q}_{\text{conv}} - \dot{Q}_{\text{evap}} - \left(c_{p,i} T_{b,3} - L_f\right) \dot{m}_{\text{ice,top}}. \end{cases} \tag{10}$$

We recall that $\dot{Q}_{\text{conv}} = h_{tc}\left(T_{rec} - T_{b,3}\right)$, where h_{tc} is the boundary layer heat transfer coefficient and T_{rec} is the recovery temperature in degree Celsius. Three equations describe the evolution of the mean fields with the first index a and b denoting bottom and upper limits of each layer, respectively, and the second the i-th layer. The temperature in each layer satisfies

$$\frac{\partial \widehat{T}_1}{\partial t} = 6\frac{\alpha_i}{h^2}\left[T_{a,1} - \left(2 + \frac{\frac{\partial h}{\partial t}h}{6\alpha_i}\right)\widehat{T}_1 + \left(1 + \frac{\frac{\partial h}{\partial t}h}{6\alpha_i}\right)T_{b,1}\right] \tag{11}$$

$$\frac{\partial \widehat{T}_2}{\partial t} = 6\frac{\alpha_i}{h^2}\left[\left(1 - \frac{\frac{\partial h}{\partial t}h}{6\alpha_i}\right)T_{a,2} - \left(2 + \frac{\frac{\partial h}{\partial t}h}{6\alpha_i}\right)\widehat{T}_2 + \left(1 + 2\frac{\frac{\partial h}{\partial t}h}{6\alpha_i}\right)T_{b,2}\right] \tag{12}$$

$$\frac{\partial \widehat{T}_3}{\partial t} = 6\frac{\alpha_i}{h^2}\left[\left(1 - 2\frac{\frac{\partial h}{\partial t}h}{6\alpha_i}\right)T_{a,3} - \left(2 + \frac{\frac{\partial h}{\partial t}h}{6\alpha_i}\right)\widehat{T}_3 + \left(1 + 3\frac{\frac{\partial h}{\partial t}h}{6\alpha_i}\right)T_{b,3}\right] \tag{13}$$

where the boundary conditions are reduced to the following:

$$-\lambda_i T'_{a,1} = \dot{Q}_{cond}, \quad \text{and} \quad \lambda_i T'_{b,3} = \dot{Q}_{in} - \left(h_{tc} + c_{p,i}\dot{m}_{\text{ice,top}}\right)T_{b,3}. \tag{14}$$

With $\dot{Q}_{in} = \dot{Q}_\beta - \dot{Q}_{evap} + h_{tc}T_{rec} + L_f\dot{m}_{\text{ice,top}}$. It can be seen that this system has $T_{a,1}$, $T_{b,1}$, $T_{a,2}$, $T_{b,2}$, $T_{a,3}$ and $T_{b,3}$ as additional unknowns. The number of unknowns can be reduced by imposing the continuity of temperature and fluxes across each inner layer. Considering the i-th layer this is translated by,

$$T_{b,i} = T_{a,i+1} \quad \text{and} \quad \lambda\frac{\partial T_i}{\partial z}\Big|_{z=h+(i-1)h} = \lambda\frac{\partial T_{i+1}}{\partial z}\Big|_{z=h+(i-1)h}. \tag{15}$$

Here we define the followings variables,

$$T_{\mathrm{p}} = \frac{\dot{Q}_{cond} h}{2\lambda_i}, \quad T_{in} = \frac{\dot{Q}_{in} h}{2\lambda_i}, \quad B_{eq} = \frac{1}{2}\frac{h}{\lambda_i}\left[h_c + c_{p,i}\dot{m}_{\mathrm{ice,top}}\right] \text{ and } \eta = 26B_{eq} + 45,$$

and with the equation (15) the interface temperatures after straightforward calculations are,

$$\begin{cases} T_{a,1} = \dfrac{\widehat{T_1}}{\eta}(57 + 33B_{eq}) - 3\dfrac{\widehat{T_2}}{\eta}(5 + 3B_{eq}) + 3\dfrac{\widehat{T_3}}{\eta}(1 + B_{eq}) + \dfrac{T_{\mathrm{p}}}{\eta}(26 + 15B_{eq}) - \dfrac{T_{in}}{\eta} \\ T_{b,1} = 3\dfrac{\widehat{T_1}}{\eta}(7 + 4B_{eq}) + 6\dfrac{\widehat{T_2}}{\eta}(5 + 3B_{eq}) - 6\dfrac{\widehat{T_3}}{\eta}(1 + B_{eq}) - \dfrac{T_{\mathrm{p}}}{\eta}(7 + 4B_{eq}) + 2\dfrac{T_{in}}{\eta} \\ T_{b,2} = -3\dfrac{\widehat{T_1}}{\eta}(2 + B_{eq}) + 15\dfrac{\widehat{T_2}}{\eta}(2 + B_{eq}) + 21\dfrac{\widehat{T_3}}{\eta}(1 + B_{eq}) + \dfrac{T_{\mathrm{p}}}{\eta}(2 + B_{eq}) - 7\dfrac{T_{in}}{\eta} \\ T_{b,3} = 3\dfrac{\widehat{T_1}}{\eta} - 15\dfrac{\widehat{T_2}}{\eta} + 171\dfrac{\widehat{T_3}}{\eta} - \dfrac{T_{\mathrm{p}}}{\eta} + 26\dfrac{T_{in}}{\eta} \end{cases} \tag{16}$$

By discretising the differential equations of the mean temperature for each layer (Eq. 11-13), taking into account the previous results, it is possible to find the system of equations (17), where the temperatures have been taken implicitly and the heights of each layer explicitly.

$$\left(\boldsymbol{I} - \Delta t \frac{\alpha_i}{h^2}\boldsymbol{A}_{\mathrm{rime}}\right)\widehat{\boldsymbol{T}}^{\,n+1} = \widehat{\boldsymbol{T}}^{\,n} + \Delta t \frac{\alpha_i}{h^2}\boldsymbol{b}_{\mathrm{rime}}. \tag{17}$$

With $\widehat{\boldsymbol{T}} = (\widehat{T_1},\ \widehat{T_2},\ \widehat{T_3})^t$, $\boldsymbol{I}$ the identity matrix, and $\boldsymbol{A}_{\mathrm{rime}}$ and $\boldsymbol{b}_{\mathrm{rime}}$ are given in appendix.

2.3 Multi-layered approach to glaze ice

The same strategy is employed for the ice layer that appears in a glaze ice accretion scenario. This time, the boundary conditions for the ice layer are

$$\begin{cases} -\lambda_i \frac{\partial T_{ice}}{\partial z}\Big|_{z=0} &= \dot{Q}_{cond} \\ T_{b,3} &= T_m = 0^o\, C. \end{cases} \tag{18}$$

Once again, this can be written as a system to solve

$$\left(\boldsymbol{I} - \Delta t \frac{\alpha_i}{h^2}\boldsymbol{A}_{\mathrm{glaze}}\right)\widehat{\boldsymbol{T}}^{\,n+1} = \widehat{\boldsymbol{T}}^{\,n} + \Delta t \frac{\alpha_i}{h^2}\boldsymbol{b}_{\mathrm{glaze}} \tag{19}$$

with $\boldsymbol{A}_{\mathrm{glaze}}$ and $\boldsymbol{b}_{\mathrm{glaze}}$ given in appendix.

2.4 Multi-layered approach to rime ice with static film

The static film is solved using the integral approach with one layer as described in section 2.1. In the ice block, the three-sublayers strategy is employed, with the boundary conditions being

$$\begin{cases} T_{a,1} = T_m &= 0^o\, C \\ \lambda_i \frac{\partial T_{ice}}{\partial z}\Big|_{z=h_i} &= \dot{Q}_\beta + \dot{Q}_{\mathrm{conv}} - \dot{Q}_{\mathrm{evap}} - \left(c_{p,i} T_{b,3} - L_f\right)\dot{m}_{\mathrm{ice,top}}. \end{cases} \tag{20}$$

The system to solve is

$$\left(\boldsymbol{I} - \Delta t \frac{\alpha_i}{h^2} \boldsymbol{A}_{\text{static/rime}}\right) \widehat{\boldsymbol{T}}^{\,n+1} = \widehat{\boldsymbol{T}}^{\,n} + \Delta t \frac{\alpha_i}{h^2} \boldsymbol{b}_{\text{static/rime}} \tag{21}$$

with $\boldsymbol{A}_{\text{static/rime}}$ and $\boldsymbol{b}_{\text{static/rime}}$ given in appendix.

2.5 Multi-layered approach to glaze ice with static film

As in the previous section, the static film is solved using the integral approach with one layer. The ice block boundary conditions corresponding to a glaze ice situation with a static film are as follows

$$\left\{ \begin{array}{lcl} T_{a,1} & = & T_m = 0^o\, C \\ T_{b,3} & = & T_m = 0^o\, C. \end{array} \right. \tag{22}$$

The corresponding system to be solved is

$$\left(\boldsymbol{I} - \Delta t \frac{\alpha_i}{h^2} \boldsymbol{A}_{\text{static/glaze}}\right) \widehat{\boldsymbol{T}}^{\,n+1} = \widehat{\boldsymbol{T}}^{\,n} + \Delta t \frac{\alpha_i}{h^2} \boldsymbol{b}_{\text{static/glaze}} \tag{23}$$

with $\boldsymbol{A}_{\text{static/glaze}}$ and $\boldsymbol{b}_{\text{static/glaze}}$ given in appendix.

2.6 Solving runback

The film thickness of runback is typically a few microns. A constant temperature model is used. The mass and energy conservation equations (1a) and (1b) are solved using an explicit finite volume scheme. The fluxes are approximated using either Roe or HLL, as selected by the user. The energy equation's source term, $\dot{Q}_{conv}$, is taken implicit along with $\dot{Q}_{ice}$ if the system is in a glaze state. It is possible to add the radiation in the energy equation, $\dot{Q}_{rad} = \sigma\epsilon\left(T_\infty^4 + (T_f + T_m)^4\right)$, with T_f in Celsius. In such a case, this radiation source term is linearized and taken implicitly.

3 NUMERICAL RESULTS

3.1 Validation using the Stefan problem

$c_i\,(JK_g^{-1}K^{-1})$	$c_w\,(JK_g^{-1}K^{-1})$	$L_f\,(JK_g^{-1})$	$\lambda_i\,(Wm^{-1}K^{-1})$	$\lambda_w\,(Wm^{-1}K^{-1})$	$T_m(K)$
2060	4185	333000	2.1	0.6	273.15

Table 1: Physical properties used for the Stefan problem simulation.

To validate the multilayer method, the Stefan problem is solved and the solution is compared with the analytical solution. The Stefan problem is a block of frost of size L initially at a temperature $T_0 = 263.15\,K$. $T_w = 283.15\,K$. The problem is 1D with adiabatic lateral edges and the ice size is large compared to the size of the melting front (semi-infinite domain). The state at the upper boundary is a mixed state similar to that encountered in icing with $h_{tc} =$

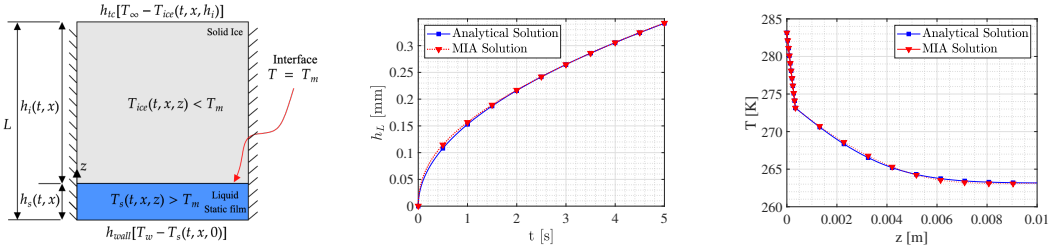

(a) Stefan problem set-up. (b) Melting front position. (c) Temperature profile $t = 5\,s$.

Figure 4: Comparison between the analytical Stefan solution and the numerical solution obtained with MIA.

$300\,W\,m^{-2}\,K^{-1}$, see Figure 4a. The interface of the melting front is a function of time $h_s(t)$ and the analytical solution is given by [4]

$$h_s(t) = 2\chi\sqrt{\alpha_w t} \tag{24}$$

χ is solution of

$$\frac{St_s}{\exp(\chi^2)\mathrm{erf}(\chi)} - \frac{St_i}{\nu\exp(\nu^2\chi^2)\mathrm{erfc}(\nu\chi)} = \chi\sqrt{\pi}, \tag{25}$$

with

$$St_s = c_{p_w}\frac{(T_w - T_m)}{L_m}, \quad St_i = c_{p_i}\frac{(T_m - T_0)}{L_m}, \quad \nu = \sqrt{\frac{\alpha_w}{\alpha_i}}.$$

In this situation, the system of equations (1) simplifies to

$$\begin{cases} T(0,z) = T_0 < T_m & t = 0, \quad \text{Initial condition} \\ \dfrac{\partial T_s}{\partial t} = \alpha_w \dfrac{\partial^2 T_s}{\partial z^2}, & 0 < z < h_s(t), \quad \text{Liquid static} \\ \dfrac{\partial T_{ice}}{\partial t} = \alpha_i \dfrac{\partial^2 T_{ice}}{\partial z^2}, & z > h_s(t), \quad \text{Solid ice} \\ T(t, h_s(t)) = T_m, & \text{Interface} \\ \dot{m}_{\text{ice}} L_f = -\lambda_w \dfrac{\partial T_s}{\partial z}\Big|_{z=h_s} + \lambda_i \dfrac{\partial T_{ice}}{\partial z}\Big|_{z=h_s}, & \text{Stefan condition} \end{cases} \tag{26}$$

In our simulation, $\Delta t = 0.001\,s$, we select one layer in the static film and three layers inside the ice block with L, the block length, initially set to $10^{-2}\,m$.

3.2 Icing configuration comparison between a uniform ice temperature and MIA

The parameters of this numerical simulation correspond to the NASA31 test case described in articles [5, 6]. They are summarized in Table 2. The air flow solution is solved with SU2

using the Sapalart-Allmaras turbulence model and the 2PP turbulent Prandtl correction [7]. A variable roughness height is defined as a function of the curvilinear abscissa s, where $k = \frac{-1}{0.058}\Big||s - s_0| - 0.045\Big|^3 + 0.0017$. The value of s_0 represents the stagnation point, and the ratio k_s/k is equal to 2.8. The parameter k_s is defined as the equivalent sand grain roughness. The parameters for k have been derived through a data-driven Bayesian calibration, as detailed in reference [5]. The corresponding convective heat transfer coefficient h_{tc} and collection efficiciency β for this case is given Figure 5a.

Airfoil	c $[m]$	T_∞ $[K]$	α $[^o]$	U_∞ $[m/s]$	P_∞ $[KPa]$	LWC $[g/m^3]$	d $[\mu m]$	ρ_{ice} $[kg/m^3]$	t $[s]$
NACA0012	0.5334	269.1	4	58.1	95.61	1.30	20	917	480

Table 2: NASA31 test case.

In this glaze ice configuration, the two numerical ice shapes and the experimental one are in good agreement. The classical SWIM approach and the proposed multi-layered integral method, using three layers inside the ice, are compared. As expected, the predicted liquid water film thickness and ice thickness match perfectly for this case, as illustrated in Figures 5c and 5b. This result demonstrates that the method does not compromises the results of more conventional approaches in cases of icing.

3.3 De-icing configuration

The deicing scenario being considered is the one described in [2]. Table 3 summarizes the main parameters. A constant roughness is used for this test case with, $k_s = k = 0.498$ mm, and the 2PP correction for the Prandtl [7]. During the initial 20 seconds of the case, internal heating is not activated. The collection efficiency and the convective heat transfer coefficient for this case are presented in Figure 6. The ice and water film thickness after 20 seconds of accretion is presented in Figure 6 right. These results are in agreement with those of Chauvin *et al.* [2]. After $20s$ of accretion, an ice protection system is activated. The heat provided by the system is represented by an internal heat transfer coefficient of $1500\,W\,K^{-1}\,m^{-2}$ and an internal temperature of $323.15K$. The system is active between $s = -0.015\,m$ and $s = 0.015\,m$. The solution is plotted at time $t = 50.01\,s$ to compare with Chauvin *et al.*'s results [2]. In the heating zone, all ice is removed and ice ridges begin to form, as illustrated in figure 7 left and right. The ice thickness is in agreement with literature results.

Airfoil	c $[m]$	T_∞ $[K]$	α $[^o]$	U_∞ $[m/s]$	P_∞ $[KPa]$	LWC $[g/m^3]$	d $[\mu m]$	ρ_{ice} $[kg/m^3]$
NACA0012	0.5334	263.15	4	104.4	101.325	0.34	20	917

Table 3: De-icing test case parameters

4 CONCLUSION

This study proposes a modification of the shallow water icing model to handle de-icing phenomena. The model applies a temperature profile, enabling the generation of a static film on the

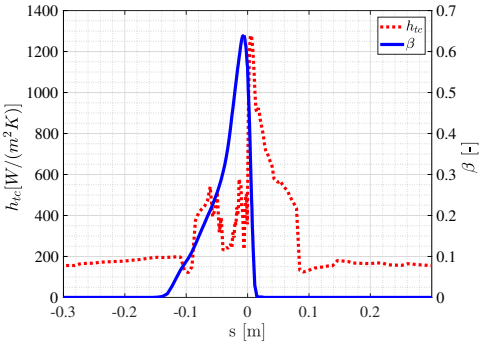

(a) Heat transfer coefficient and collection efficiency.

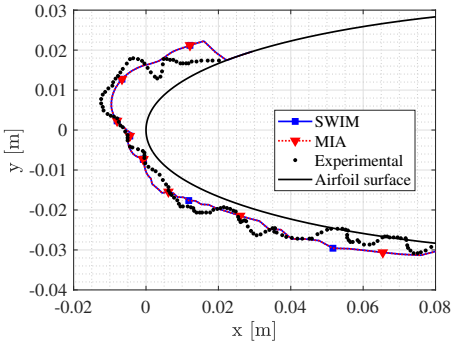

(b) Experimental and numerical ice shapes.

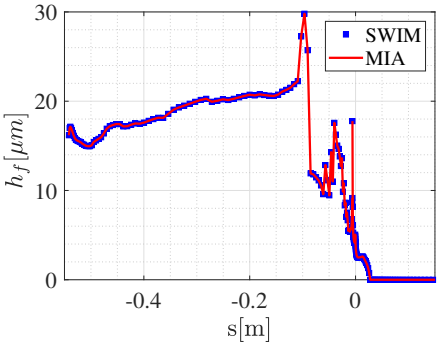

(c) Liquid film height.

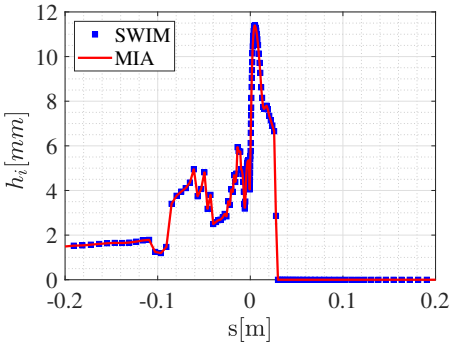

(d) Ice height.

Figure 5: NASA31 icing test case on a NACA 0012 airfoil.

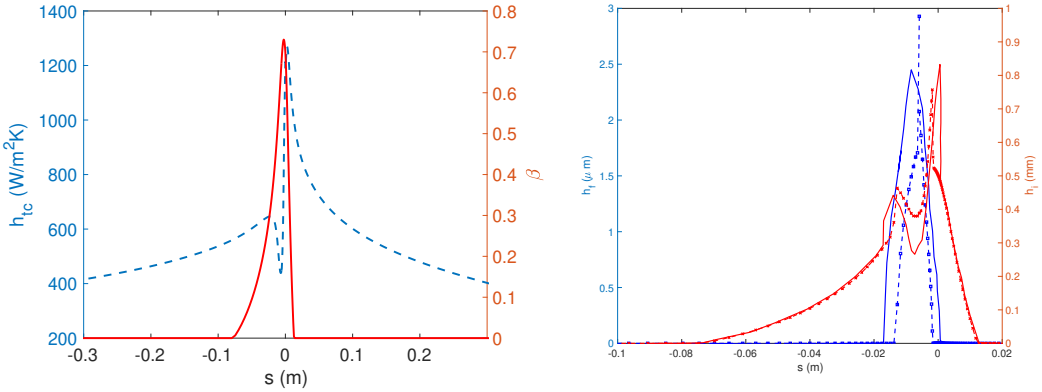

Figure 6: Left: Heat transfer coefficient and collection efficiency. Right: Ice and water film thickness after 20s, Lines: chauvin *et Al.* [2] results, dot lines with symbols: MIA results.

wall when a heat conduction source term from a thermal resistance is present. A multilayered integral approach and appropriate boundary conditions close the problem. The multilayered method is verified against the analytical solution of the Stefan problem for ice block melting.

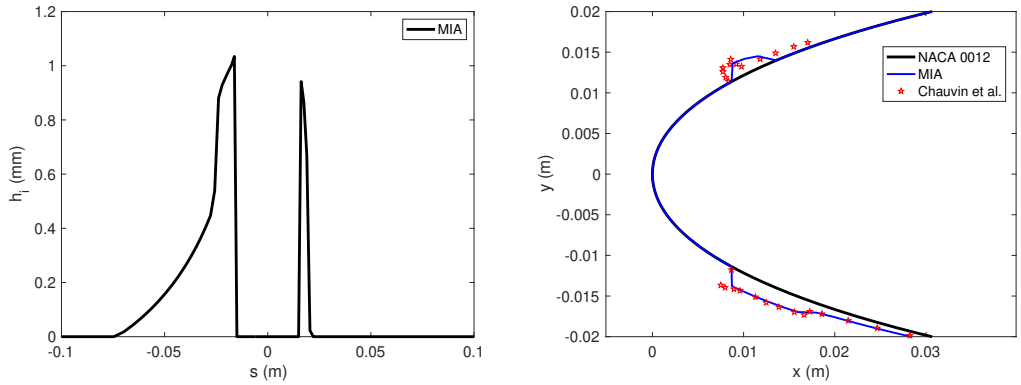

Figure 7: Deicing step, simulation lasts 50.01s. Left: Ice thickness. Right: comparison with Chauvin *et al.*, each ice thickness is double as in paper [2].

In the context of icing conditions, an iced airfoil test case successfully validate the code. In the context of de-icing conditions, the code results are verified against numerical results for an airfoil and are promising. Future work will require validation against experimental data.

A APPENDIX

We define $P = \frac{\frac{\partial h}{\partial t}h}{6\alpha_i}$. Recall that $h(t,x) = \frac{h_i(t,x)}{3}$, $T_{\mathrm{p}} = \frac{\dot{Q}_{cond}h}{2\lambda_i}$, $T_{in} = \frac{\dot{Q}_{in}h}{2\lambda_i}$, and $B_{eq} = \frac{1}{2}\frac{h}{\lambda_i}\left[h_c + c_{p,i}\dot{m}_{\mathrm{ice,top}}\right]$

$$\boldsymbol{A}_{\mathrm{xxx}} = \begin{bmatrix} a_{11} & a_{12} & a_{13} \\ a_{21} & a_{22} & a_{23} \\ a_{31} & a_{32} & a_{33} \end{bmatrix} \qquad \boldsymbol{b}_{\mathrm{xxx}} = \begin{bmatrix} b_1 \\ b_2 \\ b_3 \end{bmatrix}$$

A.1 Rime case: $\boldsymbol{A}_{\mathbf{rime}}$, $\boldsymbol{b}_{\mathbf{rime}}$

Recall that $\eta = 26B_{eq} + 45$

$$a_{11} = -\frac{(1+2P)(12+7B_{eq})}{\eta} \qquad a_{12} = 3\frac{(1+2P)(5+3B_{eq})}{\eta}$$
$$a_{13} = -3\frac{(1+2P)(1+B_{eq})}{\eta} \qquad a_{21} = -3\frac{(11P-5+(6P-3)B_{eq})}{\eta}$$
$$a_{22} = -\frac{15(2+P)+B_{eq}(19+14P)}{\eta} \qquad a_{23} = 3\frac{(5+16P)(1+B_{eq})}{\eta}$$
$$a_{31} = 3\frac{[B_{eq}(2P-1)+7P-1]}{\eta} \qquad a_{32} = -3\frac{5[B_{eq}(2P-1)+7P-1]}{\eta}$$
$$a_{33} = \frac{84P-12-(31+68P)B_{eq}}{\eta}$$

And

$$b_1 = \frac{(19-7P+(11-4P)B_{eq})T_{\mathrm{p}} + (1+2P)T_{in}}{\eta}$$
$$b_2 = \frac{(11P-5+(6P-3)B_{eq})T_{\mathrm{p}} - (5+16P)T_{in}}{\eta}$$
$$b_3 = \frac{[1-7P+B_{eq}(1-2P)]T_{\mathrm{p}} + [19+92P]T_{in}}{\eta}$$

A.2 Glaze case: $\boldsymbol{A}_{\mathbf{glaze}}$, $\boldsymbol{b}_{\mathbf{glaze}}$

In this scenario $\eta = 26$.

$$a_{11} = -\frac{7+14P}{\eta} \quad a_{12} = 9\frac{1+2P}{\eta} \quad a_{13} = -3\frac{1+2P}{\eta}$$
$$a_{21} = -9\frac{2P-1}{\eta} \quad a_{22} = -\frac{19+14P}{\eta} \quad a_{23} = 3\frac{2+10P}{\eta}$$
$$a_{31} = 3\frac{2P-1}{\eta} \quad a_{32} = -3\frac{5(2P-1)}{\eta} \quad a_{33} = -\frac{40+50P}{\eta}$$

$$b_1 = \frac{(11-4P)}{\eta}T_{\mathrm{p}}, \quad b_2 = 3\frac{(2P-1)}{\eta}T_{\mathrm{p}}, \quad b_3 = -\frac{(2P-1)}{\eta}T_{\mathrm{p}}$$

A.3 Static film + Rime: $A_{\text{static/rime}}$, $b_{\text{static/rime}}$

$$\eta = 26 + 15B_{eq}, \quad P = h\frac{\frac{\partial h}{\partial t}}{6\alpha_i}, \quad G = h\frac{\frac{\partial h_s}{\partial t}}{6\alpha_i}$$

$$a_{11} = \frac{21(1+G+P) - (2+P)\eta + 12(1+G+P)B_{eq}}{\eta}$$
$$a_{22} = \frac{3(11+G+7P) - (2+P)\eta + 9(2+P)B_{eq}}{\eta}$$
$$a_{33} = -\frac{-3(10+7G+25P) - (2+P)\eta + 9(2+P)B_{eq}}{\eta}$$
$$a_{12} = 3\frac{(1+G+P)(5+3B_{eq})}{\eta} \qquad a_{13} = -3\frac{(1+G+P)(1+B_{eq})}{\eta}$$
$$a_{21} = -3\frac{-5+9G+11P+4(2G+3P)B_{eq}}{\eta} \qquad a_{23} = 3\frac{(3+5G+9P)(1+B_{eq})}{\eta}$$
$$a_{31} = 3\frac{8+3G+7P+4(1+G+P)B_{eq}}{\eta} \qquad a_{32} = -3\frac{-2+9G+21P+3(-1+G+2P)B_{eq}}{\eta}$$

$$b_1 = (1+G+P)\frac{T_{in}}{\eta}, \quad b_2 = -(3+5G+9P)\frac{T_{in}}{\eta}, \quad b_3 = (16+19G+53P)\frac{T_{in}}{\eta}$$

A.4 Static film + Glaze: $A_{\text{static/glaze}}$, $b_{\text{static/glaze}}$

$$\eta = 5, \quad G = \frac{\frac{\partial h_s}{\partial t}h}{6\alpha_i}$$

$$a_{11} = \frac{4G-P-6}{\eta} \quad a_{12} = 3\frac{1+G+P}{\eta} \quad a_{13} = -3\frac{1+G+P}{\eta}$$
$$a_{21} = \frac{3-5G-6P}{\eta} \quad a_{22} = -\frac{4+2P}{\eta} \quad a_{23} = \frac{1+7G+11P}{\eta}$$
$$a_{31} = \frac{G+2P-1}{\eta} \quad a_{32} = -3\frac{(G+2P-1)}{\eta} \quad a_{33} = -\frac{6+4G+13P}{\eta}$$

$$b_1 = b_2 = b_3 = 0$$

REFERENCES

[1] Y. Bourgault, H. Beaugendre and W. G. Habashi. Development of a shallow-water icing model in FENSAP-ICE. *Journal of Aircraft*, **37**:640-646, 2000. https://doi.org/10.2514/2.2646.

[2] R. Chauvin, L. Bennani, P. Trontin and P. Villedieu. An implicit time marching Galerkin method for the simulation of icing phenomena with a triple layer model. *Finite Elements in Analysis and Design*, **150**:20–33, 2018. https://doi.org/10.1016/j.finel.2018.07.003.

[3] L. Bennani, P. Trontin and E. Radenac. Numerical simulation of an electro-thermal ice protection system in anti-icing and de-icing mode. *Aerospace*, **10**(**1**), 2023. https://doi.org/10.3390/aerospace10010075.

[4] V. Alexiades and A.D. Solomon. Mathematical Modeling of Melting and Freezing Processes, *Taylor & Francis*, 1993.

[5] K. Ignatowicz, F. Morency and H. Beaugendre. Data-driven Roughness Estimation for Glaze Ice Accretion Simulation, *SAE Technical Paper 2023-01-1449*, 2023. https://doi.org/10.4271/2023-01-1449.

[6] K. Ignatowicz, H. Beaugendre and F. Morency. Numerical Simulation of In-Flight Iced Surface Roughness, *Handbook of Numerical Simulation of In-Flight Icing*, Springer Nature, 2023, https://doi.org/10.1007/978-3-030-64725-4_29-1.

[7] F. Morency and H. Beaugendre. Comparison of turbulent Prandtl number correction models for the Stanton evaluation over rough surfaces, *International Journal of Computational Fluid Dynamics*, 2020. doi 10.1080/10618562.2020.1753712.